TOWARDS PAIN CONTROL BY MODELING THE INTERACTIONS IN A MAMMALIAN NERVE FIBER

by

Vijay Sadashivaiah

A thesis submitted to Johns Hopkins University in conformity with the requirements for the degree of Master of Science in Engineering

Baltimore, Maryland

May 2017

Abstract

Objectives. Electrical stimulation of nerve fibers is used to treat various diseases. Despite efforts to model the effects of stimulation, its underlying mechanisms remain unclear. This is because current mechanistic models just quantify the effects that the electrical field produces near the fiber and do not capture interactions between stimulus-initiated action potentials (APs) and underlying physiological activity initiated APs. Physiological activity induced APs, noxious or innocuous, travel along the fibers and may, for example, collide with a stimulus AP, and thus may never be relayed to the brain. In this study, we aim to quantify the effects of stimulation frequency on these interactions.

Methods. We construct three computational models of a nerve fiber of varying degrees of complexity (probabilistic, reduced and mechanistic) each receiving two inputs: the underlying physiological activity at one end of the fiber, and the external stimulus applied to the middle of the fiber. We then define relay reliability, R, as the percentage of physiological APs that make it to the other end of the nerve fiber. We apply the two inputs to the fiber at various frequencies and analyze relay reliability.

Results. We find that at input frequencies ($< 50\,\mathrm{Hz}$), both reduced and mechanistic models generate similar relay maps, and interactions are mainly due to collisions and inter-signal loss of excitability (stimulus AP induces refractory period and thus fiber does not respond to a physiological input and vice-versa). Higher frequency ($> 100\,\mathrm{Hz}$) inputs result in intra-signal loss of excitability (stimulus/physiological AP

induces refractory period and fiber does not respond to next stimulus/physiological pulse). The interaction statistics produced by reduced versus mechanistic models are linearly related. On the other hand, the probabilistic model captures relay properties for low input frequencies ($< 10\,\mathrm{Hz}$) but then differs from reduced and mechanistic models if either input has a larger frequency. This is because the probabilistic model only accounts for only (i) inter signal loss of excitability and (ii) collisions between stimulus-initiated action potentials (APs) and underlying physiological activity initiated APs.

Conclusions. Modeling the interactions in a nerve fiber opens up opportunities towards understanding mechanisms of electrical stimulation therapies.

Thesis Committe

Dr. Sridevi V. Sarma (Advisor)

Associate Professor

Department of Biomedical Engineering

Johns Hopkins University

Dr. Yun Guan

Associate Professor

Department of Anesthesiology and Critical Care Medicine

Johns Hopkins Medical Institute

Dr. William S. Anderson

Associate Professor

Department of Neurosurgery

Johns Hopkins Medical Institute

Acknowledgements

First of all, I would like to express my sincere gratitude to my advisor, Dr. Sridevi S. Sarma for the continuous support, guidance and motivation throughout my Master's studies. Her enthusiasm and positive encouragement have influenced my desire to pursue PhD studies and I truly could not have imagined having a better advisor and mentor.

Besides my advisor, I would like to thank my other mentors, Dr. Pierre Sacré, Dr. Yun Guan and Dr. William S. Anderson for contributing their time and expertise throughout the project. Their insightful comments and feedback, and always positive attitude, were critical to the success of this thesis. I am grateful to have had the opportunity to work with such an amazing team of mentors.

I would also like to acknowledge the faculty involved in the Biomedical Engineering Master's Program at Johns Hopkins. Special thanks to Mr. Samuel Bourne for all his suggestions and help during the past two years.

I am extremely thankful for all the new friendships I have made during my Master's studies. I want to thank all my friends in Baltimore for sharing this journey with me, through the good times and the tough times, and for all the fun we had together. The past two years would not have been the same without them.

Most importantly I want to thank my parents, my brother and Nidhi for always believing in me and for their endless love and support. Without their patience, understanding and encouragement I never would have made it through ...

Contents

List of Figures

List of Tables

1 Introduction

1.1 Context

Studying the effects of electrical stimulation on mammalian nerve fibers has been of prime interest due to its applications in treating various diseases. Stimulation of peripheral and dorsal column fibers is used to alleviate acute and chronic pain (Shealy *et al* 1967, Wall and Sweet 1967, Stidd *et al* 2012, Shechter *et al* 2013); stimulation of muscle fibers is used to restore sensory or motor function loss caused by nerve injury or disease such as multiple sclerosis and cerebral palsy (Kralj and Bajd 1989, Pfurtscheller *et al* 2003, Peckham and Kilgore 2013); and stimulation of the vagus nerve has been effective in treating epilepsy, depression, and anxiety (Groves and Brown 2005). In many cases, these nerve fibers have ongoing physiological activity that interacts with the exogenous activity generated by the external current stimulus. For example, when a splinter pricks your toe, a pain sensor called a nociceptor sends an action potential (AP) up your leg through nerve fibers to a cluster of cells in the spinal cord. The cluster of cells output modulated pain signals up to the brain through fibers that may also transmit APs induced by dorsal column stimulation. That is, the antidromic APs induced by stimulation moving down the fibers interact with the physiological activity moving up the same fibers.

There are three main interactions: (i) *collision block* due to annihilation of antidromic stimulus initiated APs with orthodromic APs from ongoing physiological activity, (ii) *inter signal loss of excitability* of fiber by ongoing physiological activity initiated

AP due to recent stimulus AP (physiological–stimulus), and vice versa (stimulus–physiological), (iii) *intra signal loss of excitability* of the fiber by stimulus initiated AP due to recent stimulus AP (stimulus–stimulus) and by ongoing physiological activity initiated AP due to recent ongoing physiological activity AP (physiological–physiological). We have not considered phase resetting Crago and Makowski (2014) as a part of this study but plan to include in the future work. In order to better understand and optimally design stimulation therapies for diseases, it is necessary to understand when and how often each of these interactions occur under different stimulation protocols.

1.2 Need

There have been computational efforts to study excitability and interactions in a mammalian nerve fiber. Over the past few decades, bio-physical conductance based models of nerve fibers have been developed to study their excitability properties (Reilly 1989, Wesselink *et al* 1999, McIntyre *et al* 2002) to name a few. These studies characterize the effects of stimulation on the fiber, such as activation threshold and conduction velocity, by modeling different nerve geometries (single cable or double cable), different tissue mediums, and different electrode configurations, but do not study interactions between stimulus generated APs with ongoing physiological activity in the fiber.

A more recent study developed a simple computational model based on speed of conduction and refractory periods to capture these interactions (Crago and Makowski 2014). Two inputs were applied: (i) the physiological activity modeled as a spike train whose mean firing rate is generated by a normal distribution and (ii) the external stimulus modeled as a periodic train of APs, that was applied to different sites along the fiber. Collision block and inter signal loss of excitability were studied as a function of the mean firing rate of physiologically-generated APs. This reduced

model is the first to investigate interactions rigorously but cannot identify nonlinear effects that may arise in the biophysical fiber system. Furthermore, ongoing physiological activity is highly varying which may not be well characterized by a normally distributed firing pattern (Jänig *et al* 2009). Similarly, variable patterns (bursts, Poisson, etc.) of stimulus are more realistic characterizations of physiological response processes (Bruns *et al* 2009).

1.3 Task

In this study, we characterized all three types of interactions between antidromic APs generated by a deterministic periodic external stimulus and orthodromic physiological APs generated by a stochastic Poisson process. Specifically, we constructed three models of varying degrees of complexity (probabilistic, reduced and mechanistic) of a single nerve fiber. The *probabilistic model* is a simple model that captures the probability of a physiological AP reaching the other end of nerve fiber based on length of nerve fiber (l), speed of conduction (c) and refractory periods. The *reduced model* is a simple model of a myelinated nerve fiber that captures the interactions based on activation thresholds, speed of conduction, and refractory periods as in (Crago and Makowski 2014). The *mechanistic model* is a detailed model of single cable nerve fiber that captures high resolution action potential interactions based on biophysical principles. The mechanistic model is constructed to assess the validity of reduced model, which was proposed in (Crago and Makowski 2014). In each model, the nerve fiber receives two inputs: the ongoing physiological activity at one end of the fiber and the external stimulus applied to the middle of the fiber (see Figure 2.1). We then compute *relay reliability*, defined as the ratio of number of physiological APs that make it to the other end of the fiber over the total number of physiological APs entering nerve fiber. Relay reliability depends on stimulus and physiological activity signal parameters including but not limited to frequency, amplitude and pattern (tonic vs bursting vs stochastic). In this study, we vary the

frequency of the input signals and analyze relay reliability under different fiber diameters.

1.4 Object

Our results suggest that at stimulus and physiological frequencies ($< 50\,\mathrm{Hz}$), the reduced model (runtime of the order of minutes) and the mechanistic model (runtime of the order of days) have similar reliability properties, but the reduced model significantly decreases the computational complexity and simulation run time. On the other hand the probabilistic model (runtime of the order of seconds) has similar reliability properties for frequencies $< 10\,\mathrm{Hz}$. At low input signal frequencies, interactions in the fiber are mainly due to collisions and inter signal loss of excitability. On the other hand, at high frequencies the interactions are mainly due to intra signal loss of excitability. The interaction statistics produced by reduced versus mechanistic models are linearly related under all input frequencies, which suggests that the reduced model captures relevant qualitative features of interactions along the fiber. Finally, increasing the axon diameter increases relay reliability for all input frequencies.

This study demonstrates that complex interactions occur between physiological and electrical stimulus along the nerve fibers and it may be useful to characterize these interactions to better understand the mechanisms of action of electrical stimulation used to treat diseases of the nervous system.

2 Methods

2.1 Mechanistic model of a nerve fiber

Methods used in this section are derived from (Sacré *et al* 2015). Here, we describe our simulation test bed of extracellular electrical stimulation on myelinated nerve fibers *with* underlying physiological activity (see Figure 2.1). The model is fairly simple: this is both an asset (in the mathematical analysis) and a limitation (in the detailed modeling of more complex structures). As our main interest is to study the effect of interactions between stimulation-evoked and underlying activities, this model provides a starting point toward the elucidation of realistic mechanisms.

2.1.1 Myelinated nerve fiber.

A myelinated nerve fiber is a cylindrical active membrane (axon), tightly wrapped in an insulating myelin sheath. This myelin sheath is interrupted periodically, leaving short gaps where the axonal membrane is exposed. Following McNeal's model (McNeal 1976), a myelinated nerve fiber is represented by an (infinite) series of compartment elements linked by intracellular conductances. The dynamics of the membrane potential $V_i = V_i^{\text{int}} - V_i^{\text{ext}}$ at node i (where V_i^{int} and V_i^{ext} are the intracellular and extracellular potentials) read as follows

$$C_{\text{m}}\,\dot{V}_i + \sum_{k\in\mathcal{K}} I_{i,k} = G_{\text{a}}\left(V_{i-1} - 2\,V_i + V_{i+1}\right) + G_{\text{a}}\left(V_{i-1}^{\text{ext}} - 2\,V_i^{\text{ext}} + V_{i+1}^{\text{ext}}\right),$$

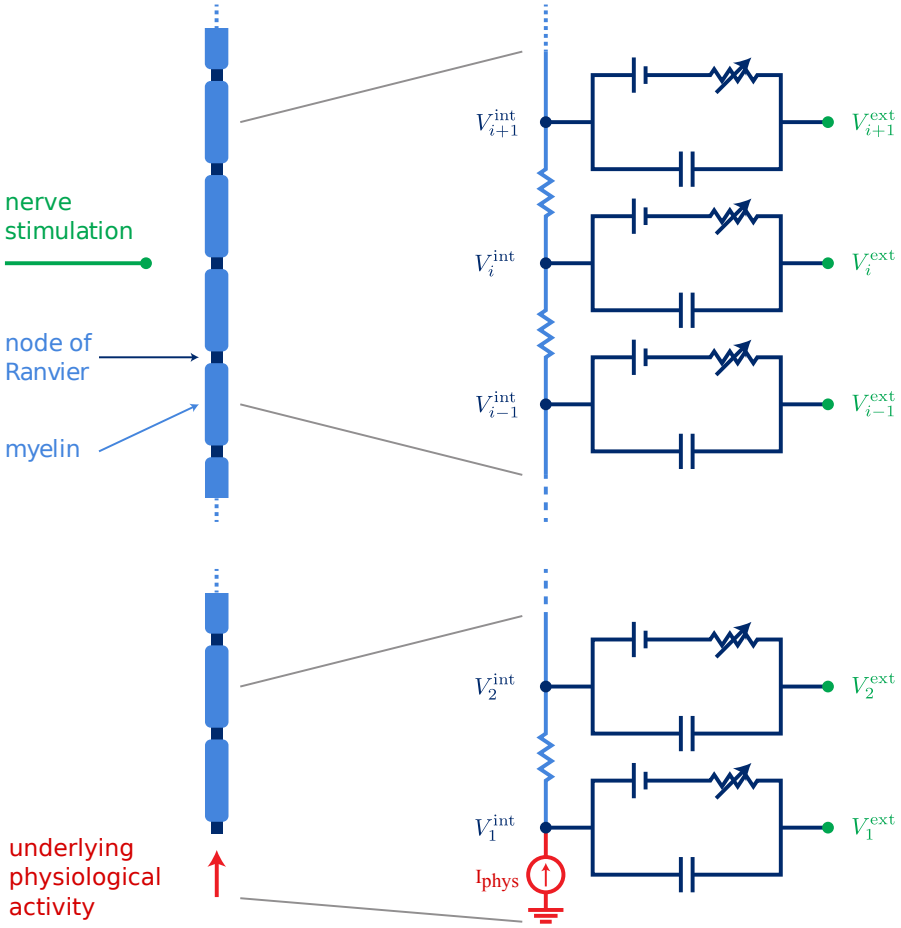

FIGURE 2.1: Mechanistic model of nerve fiber. Our model of extracellular electrical stimulation of myelinated nerve fibers includes the underlying physiological activity as a current source at one end of the nerve fiber.

where C_m is the membrane capacitance and G_a is the internodal conductance. Ionic currents $I_{i,k}$ at node i include a sodium, a fast potassium, and a slow potassium ion channel, as well as a leakage current across the membrane based on the Frankenhaeuser–Huxley model (Frankenhaeuser and Huxley 1964), adjusted to experimental data of human sensory fibers at 37 °C (Schwarz *et al* 1995). A complete description of the fiber model and its parameters is presented in (Schwarz *et al* 1995, Wesselink *et al* 1999).

To numerically compute the response of a *finite* fiber, it is usually assumed that no intracellular axial current flows at the end nodes ('sealed-end' boundary condition) (Rubinstein 1993).

2.1.2 Electrical field potential generated by stimulation.

The extracellular medium surrounding a nerve fiber is composed of different regions (epidural fat, cerebrospinal fluid, white matter, grey matter), which have different conduction properties (Struijk *et al* 1991). In addition, the electrode can also take various shapes (single contact or array of contact) and various configurations (monopolar, bipolar, or other) (Medtronic Neuromodulation 2007). However, the extracellular medium may be assumed to be infinite and isotropic with the electrode represented by point sources at the center x_j^c of each contact. Therefore, the electrical potential field at time t and position x is given by

$$\varphi(t,x) = \sum_{j\in\mathcal{C}} \frac{\rho_\mathrm{m}}{4\,\pi\,\|x - x_j^\mathrm{c}\|_2}\, I_j^\mathrm{stim}(t)\,,$$

where I_j^stim is the current of point source j and ρ_m is the extracellular medium resistivity. The extracellular potential at node i is given by $V_i^\mathrm{ext}(t) = \varphi(t, x_i)$, where x_i is the position of node i.

2.1.3 Underlying physiological activity.

The underlying physiological activity in fibers spans a broad frequency range and exhibits various patterns (Kajander and Bennett 1992): regular spike discharge, regular discharge of doublet spikes, bursting patterns, sporadic activity with no regular or predictable firing pattern, etc.

The presence of underlying activity in the nerve fiber is represented by replacing a 'sealed-end' boundary condition by a current source at one end of the nerve fiber. Therefore, the dynamics of the first node becomes

$$C_{\mathrm{m}}\,\dot{V}_1 + \sum_{k\in\mathcal{K}} I_{1,k} = G_{\mathrm{a}}\,(V_2 - V_1) + G_{\mathrm{a}}\left(V_2^{\mathrm{ext}} - V_1^{\mathrm{ext}}\right) + I^{\mathrm{phys}}(t)\,,$$

where the input $I^{\mathrm{phys}}(t)$ represents the underlying activity.

2.2 Reduced model of a nerve fiber

In this section, we describe our reduced model wherein the nerve fiber is characterized by its geometry (length and diameter) and three macroscopic properties: activation threshold, conduction velocity, and refractory period of the fiber. These macroscopic properties can be estimated either from biological experiments or from our high-dimensional conductance-based model. It is assumed that:

- A stimulation or physiological input creates an action potential in the fibers if and only if its amplitude is larger than the associated threshold and its timing is not within the refractory period of a preceding action potential;
- A stimulation generated action potential propagates in the fiber in both directions (orthodromic and antidromic) at a constant velocity (the conduction velocity);

- The interaction of an orthodromic physiologically-induced AP and antidromic AP induced by stimulation results in a collision, i.e., the annihilation of both action potentials.

Based on these characteristics, we can identify the interactions occurring in the fiber based only on the timing of physiological and stimulation pulses (Gonzalez-Perez *et al* 2014).

2.2.1 Interactions between stimulation induced and underlying physiological activity

We identified different types of interactions occurring between simulation-evoked activity and underlying physiological activity. In Figure 2.2, each panel represents a typical scatter plot for each interaction type. In these panels, a dot is an AP at node position z along the fiber and at time t. The stimulation input triggers the orthodromic and antidromic propagations of an AP wave (green dots) from the stimulation position at the fiber center toward the fiber ends. The physiological input triggers the orthodromic propagation of an AP wave (red dots) from one end to the other end of the fiber. Gray dots indicate the fiber response of each input in the absence of the other, that is, artificially without interaction (e.g., if no collision occurs and the APs just cross each other). The interaction type depends on the timing of both inputs generating these activities.

- A *collision* occurs when the orthodromic physiological AP wave and the antidromic stimulation-evoked AP wave meet and cancel each other. It happens if a physiological pulse is triggered slightly before or after a stimulation pulse, that is, $t_j^{\text{phys}} \in [t_i^{\text{stim}} - \Delta t_-^{\text{col}}, t_i^{\text{stim}} + \Delta t_+^{\text{col}})$.
- A *phys–stim loss of excitability* occurs when the stimulation input doesn't excite the nerve fiber due to the recent passage of the orthodromic physiological AP

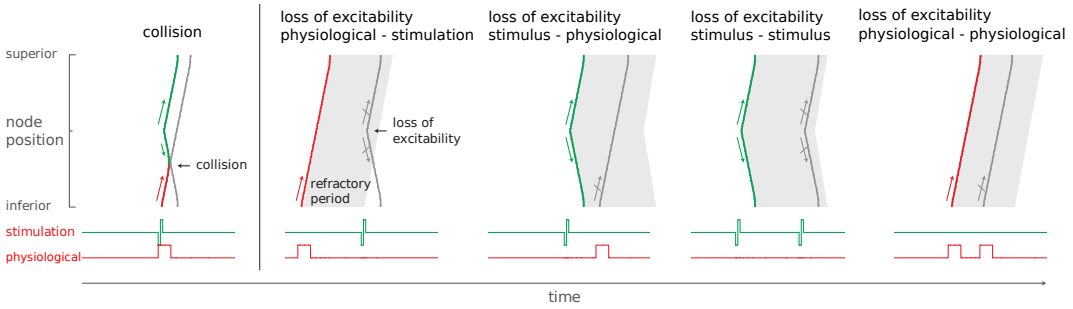

FIGURE 2.2: Different interactions between stimulation-evoked activity and physiological activity are illustrated by their scatter plots (horizontal axis is time, vertical axis is position along the nerve fiber). Each dot corresponds to an action potential at a given time t and position z along the fiber. Red and green dots indicate the fiber response to physiological and stimulation inputs, respectively. Physiological action potential waves travel orthodromically from one end to the other end of the fiber; stimulation-evoked action potential waves travel orthodromically and antidromically from the center to the extremities of the fiber. Gray dots indicate the fiber response in the absence of interactions (collision or loss of excitability), that is, the action potential wave that would be produced by the corresponding input if it was not perturbed by the activity induced by another input.

wave. It happens if a physiological pulse is triggered before a stimulation pulse, that is, $t_j^{\text{phys}} \in [t_i^{\text{stim}} - \Delta t_-^{\text{col}} - \Delta t^{\text{I}}, t_i^{\text{stim}} - \Delta t_-^{\text{col}})$.

- A *stim–phys loss of excitability* occurs when the physiological input doesn't excite the nerve fiber due to the recent passage of the antidromic stimulation-evoked AP wave. It happens if a physiological pulse is triggered after a stimulation pulse, that is, $t_j^{\text{phys}} \in [t_i^{\text{stim}} + \Delta t_+^{\text{col}}, t_i^{\text{stim}} + \Delta t_+^{\text{col}} + \Delta t^{\text{II}})$.

In addition to these interactions, we also identify 'self-interactions' or 'intra-signal' loss of excitability, that is, interactions between activities generated by the same input.

- A *stim–stim loss of excitability* occurs when the stimulation input doesn't excite the nerve fiber due to the recent stimulation of the fiber. It happens if the frequency of stimulation is too high, that is, $t_{j+1}^{\text{stim}} \in [t_j^{\text{stim}} + \Delta t^{\text{III}})$.

- A *phys–phys loss of excitability* occurs when a physiological input doesn't excite

the nerve fiber due to a recent physiological input. It happens if two consecutive Poisson pulses arrive too close to each other, that is, $t_{j+1}^{\text{phys}} \in [t_j^{\text{phys}} + \Delta t^{\text{IV}})$.

2.3 Probabilistic model of a nerve fiber

In this section, we describe our probabilistic model of nerve fibers. In this model, the nerve fiber is characterized by the geometry (length(l)) and speed of conduction (c). Using these properties we compute the probability of different events along the fiber. We assume that:

- The underlying physiological activity follows a poission distribution (rate = λ_{phys}) and the extracellular stimulus is periodic (frequency = T_{stim});
- The interactions are collisions and physiological to stimulus loss of excitability only (Including other interactions is a part of future work);

By probability theory we have,

$$P(n\ phys.\ AP\ in\ \triangle t) = \frac{e^{-\lambda \triangle t}(\lambda \triangle t)}{n!} \tag{2.1}$$

$$P(0\ phys.\ AP\ in\ \triangle t) = e^{-\lambda \triangle t} \tag{2.2}$$

$$P(At\ least\ 1\ phys.\ AP\ in\ \triangle t) = 1 - e^{-\lambda \triangle t} \tag{2.3}$$

$$Number\ of\ AP\ in\ \triangle t = \triangle t \lambda \tag{2.4}$$

Under these we compute the reliability as,

$$R_t = \frac{Number\ of\ relayed\ phsyiological\ APs}{Total\ number\ of\ physiological\ APs(T)} \tag{2.5}$$

$$= \frac{nT_{stim}\lambda_{phys} - n\ P(collision)}{nT_{stim}\lambda_{phys}} \tag{2.6}$$

We can derive the $P(collision)$ to be,

$$P(collision) = 1 - P(no\ collision) \tag{2.7}$$

$$P(no\ coll.) = P(no\ coll.|\overline{ES\ AP})\ P(\overline{ES\ AP}) + P(no\ coll.|ES\ AP)\ P(ES\ AP) \tag{2.8}$$

Where ES AP referes to the action potential produced by the electrical stimulation.

$$P(no\ coll.|\overline{ES\ AP}) = 1 \tag{2.9}$$

$$\begin{aligned} P(\overline{ES\ AP}) &= P(at\ least\ one\ phys\ AP\ in\ [-r_{phys-stim}, 0]) && (2.10)\\ &= 1 - P(0\ phys\ AP\ in\ [-r_{phys-stim}, 0]) && (2.11)\\ &= 1 - e^{-\lambda r_{phys-stim}} && (2.12) \end{aligned}$$

$$\begin{aligned} P(no\ coll.|ES\ AP) &= P(0\ phys\ AP\ in\ [-l/c, l/c]) && (2.13)\\ &= e^{-\lambda \frac{2l}{c}} && (2.14) \end{aligned}$$

$$\begin{aligned} P(ES\ AP) &= P(0\ phys\ AP\ in\ [-r_{phys-stim}, 0]) && (2.15)\\ &= e^{-\lambda r_{phys-stim}} && (2.16) \end{aligned}$$

Thus we have P(no collision),

$$\begin{aligned} Pr(no\ collision) &= 1(1 - e^{-\lambda r_{phys-stim}}) + e^{-\lambda \frac{2l}{c}} e^{-\lambda r_{phys-stim}} && (2.17)\\ &= 1 - e^{-\lambda r_{phys-stim}} + e^{-\lambda \frac{2l}{c}} e^{-\lambda r_{phys-stim}} && (2.18) \end{aligned}$$

$$\begin{aligned} Pr(collision) &= 1 - P(no\ collision) && (2.19)\\ &= e^{-\lambda r_{phys-stim}}(1 - e^{-\lambda \frac{2l}{c}}) && (2.20) \end{aligned}$$

TABLE 2.1: Amplictude of physiological and stimulus inputs for mechanistic model simulations. These values were derived by stimulating the mechanistic nerve fiber of different diameters with incremental thresholds.

	6 µm	9 µm	12 µm
Physological input amplitude (nA)	5.0	6.0	7.0
Stimulus input amplitude (mA)	-2.5	-2.0	-1.8

where $r_{phys-stim}$ is the refractory period in nerve fiber due to a recent physiological AP.

2.4 Simulation protocols.

The stimulation current input $I^{\text{stim}}(t)$ consists of the repetition, at a constant frequency, f^{stim}, of symmetrical biphasic pulses with an amplitude ranging from 1.8–$2.5\,\text{mA}$ (increasing activation thresholds as fiber diameter increases, see Table 2.1) and a duration of $350\,\mu\text{s}$ (Mortimer and Bhadra 2004). We consider stimulation frequencies ranging from 1–$50\,\text{Hz}$ (Simulations in supplementary section have stimulation frequencies ranging 1–$200\,\text{Hz}$).

As a first step, the underlying physiological activity input $I^{\text{phys}}(t)$ is modeled as a Poisson train of square pulses with an amplitude of 4–$7\,\text{nA}$ (increasing activation thresholds as fiber diameter increases) and a duration of $1\,\text{ms}$. Therefore, the instantaneous firing rate λ^{phys} is assumed constant, ranging from 1–$50\,\text{Hz}$, a typical range for motor and sensory firing activity (Katz 1950, De Luca *et al* 1982). (Simulations in supplementary section have instantaneous firing rate λ^{phys} ranging 1–$200\,\text{Hz}$).

2.5 Relay reliability

When stimulation is applied to a nerve fiber, it ultimately is interfering with the ongoing physiological activity that travels from one end of the fiber to the other. To succinctly quantify the effects of stimulation on the fiber activity, we wanted

to capture how the stimulation influences the physiologically generated APs that make it to the other end of the fiber. To quantify the effects of stimulation on the nerve fiber, we define the following relay reliability metric:

$$R^{\text{phys}}(\lambda^{\text{phys}}, f^{stim}) = \frac{\text{\# of relayed physiological APs}}{\text{total \# of physiological APs}}, \tag{2.21}$$

where relayed action potentials are underlying physiological inputs that travel from one end to the other end of the fiber. This Metric (2.21) captures the effect that the stimulation has on the ongoing physiological activity. If $R = 1$ then the stimulation has no effect, and if $R = 0$, then the stimulation blocks all physiological activity from transmitting to the brain.

We may also be interested in understanding the stimulation induced orthodromic APs that make it to the other end of the fiber. These analyses are presented in supplementary material.

3 Results

3.1 Reduced vs Mechanistic

In this section, we show results of our stimulation test beds for a monopolar electrode placed $3.5\,\mathrm{mm}$ from the center of a $10\,\mathrm{cm}$-long nerve fiber. We consider three different diameters of nerve fibers in our simulations (6, 9 and $12\,\mu\mathrm{m}$). Model parameters are listed for each diameter in Table 3.1. The results presented in this section are drawn from 50 simulations for each frequency pair (physiological, stimulus) of this model with a stochastic Poisson physiological input. These results are generated by running Monte Carlo simulations, that is, running the same simulation multiple times for different realizations of the stochastic input and computing statistics (mean and standard deviation) of relay reliability. All the mechanistic model simulations were performed on NEURON simulation environment (Hines and Carnevale

TABLE 3.1: Reduced-model parameters computed from the high-dimensional conductance-based model. These values are computed by stimulating the mechanistic model with physiological and electrical stimuli derived in Table 1.

	Fiber diameter (μm)		
	6	9	12
speed of AP conduction ($\mathrm{m\,s^{-1}}$)	41.66	66.67	90.91
phys–phys refractory period (ms)	3.2	3.5	4.0
stim–stim refractory period (ms)	8.5	7.0	6.2
phys–stim refractory period (ms)	9.5	7.8	7.7
stim–phys refractory period (ms)	4.3	3.9	4.3
nerve fiber length (cm)	10	10	10
simulation time (s)	30	30	30
number of realizations (–)	50	50	50

1997). Analysis of data and reduced model simulations were performed on MATLAB, MathWorks. Individuals interested in reproducing the results of this study or using these models in their own work can find the necessary files here (Sadashivaiah 2016).

3.1.1 Relay reliability

First, we simulated a range of stimulus and physiological frequencies (1–50 Hz) whose results can be displayed in a "relay map". Using the refractory periods and the speed of conduction values from the mechanistic model, we then repeated the simulations on a reduced model of the same fiber.

3.1.2 Underlying physiological relay.

Figure 3.1 shows examples of a physiological relay map for reduced and mechanistic model for three different diameters (6, 9 and 12 µm). We see that at low stimulation and physiological frequencies (1–10 Hz), reliability is almost 1 (100%). As the stimulus frequency increases, reliability decreases. Also, the reduced model captures relay properties that the mechanistic model captures in significantly less run time and with less computational power. Although the values at each data point are different for the reduced vs mechanistic model, the overall trends are consistent across different fiber diameters.

Supplementary Figure S1 shows the relay maps for stimulus and physiological frequencies of 1–200 Hz. The relay maps for reduced and mechanistic models are very similar for low input frequencies (< 50 Hz) and begin to differ at higher stimulus frequencies (> 100 Hz). We also observe a band of frequencies spanning 5–10 Hz, where relay reliability approaches zero (For example, in Figure S1(e,f), this band is around 150 Hz stimulus frequency).

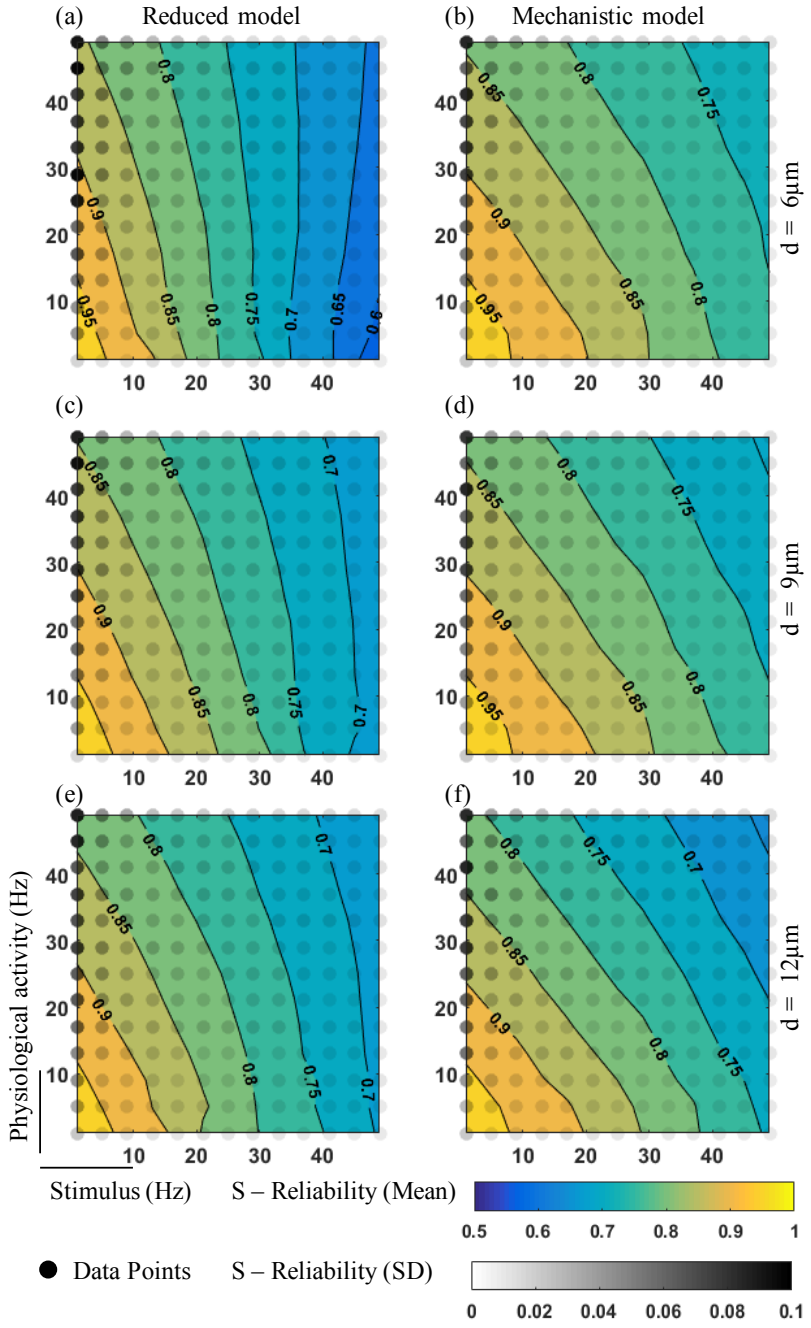

FIGURE 3.1: Physiological reliability maps of reduced and mechanistic model for 6, 9 and 12 µm diameters. Contour map of reliability values for a range (1–50 Hz) of physiological frequency (Y-axis) and stimulus frequency (X-axis). Black dots represent the data points. Color gradient represents the mean of reliability values (0.5–1). Grayscale gradient represents the standard deviation (SD) of reliability values (0–0.1).

Figure 3.2(a) quantifies the difference between the reduced and mechanistic model physiological relay maps for $9\,\mu\mathrm{m}$ diameter nerve fiber (See supplementary Figure S2 (a) for 1–$200\,\mathrm{Hz}$ stimulation). We see that for stimulus frequency lower than $25\,\mathrm{Hz}$, the difference in relay reliability between the mechanistic and reduced model is very small (< 0.04). As the stimulus frequency increases above $25\,\mathrm{Hz}$, the difference increases.

3.1.3 Influence of fiber diameter on relay reliability

Figure 3.1 shows that for different fiber diameters, the relay maps change. We observe a horizontal shift in the pattern as we go from 6–$12\,\mu\mathrm{m}$ diameter fibers. Consider a stimulus frequency of $50\,\mathrm{Hz}$ and physiological frequency of $10\,\mathrm{Hz}$, we see that the relay values for $12\,\mu\mathrm{m}$ is greater than that of $9\,\mu\mathrm{m}$ which is greater than $6\,\mu\mathrm{m}$ ($12\,\mu\mathrm{m} > 9\,\mu\mathrm{m} > 6\,\mu\mathrm{m}$). This is because of the low conduction velocity of AP's in small fibers. With an increase in fiber diameter, relay reliability increases as the interactions are reduced at higher conduction velocities. Figure 3.2(b,c) shows the difference between the relay maps of $6\,\mu\mathrm{m}$ and $12\,\mu\mathrm{m}$ diameter fibers for reduced and mechanistic models (See supplementary Figure S2(b,c) for 1–$200\,\mathrm{Hz}$ stimulation).

3.1.4 Interaction statistics

Consider the relay maps for $9\,\mu\mathrm{m}$ nerve fiber (see Figure 3.3(a,b)). Here, we have 5 different locations on the map labeled 1 to 5. Each corresponding image shows a bar plot of the interactions involved at the marked location. Except for collisions, we see that the interaction count is similar between the reduced and mechanistic model. The reduced model captures more collisions than the mechanistic model. There are no stimulus–stimulus loss of excitability since the stimulus frequency is not high enough. The percentage of action potentials reaching the other end of the fiber due to (i) stimulus and (ii) underlying physiological activity is represented in Figure 3.3c. In summary,

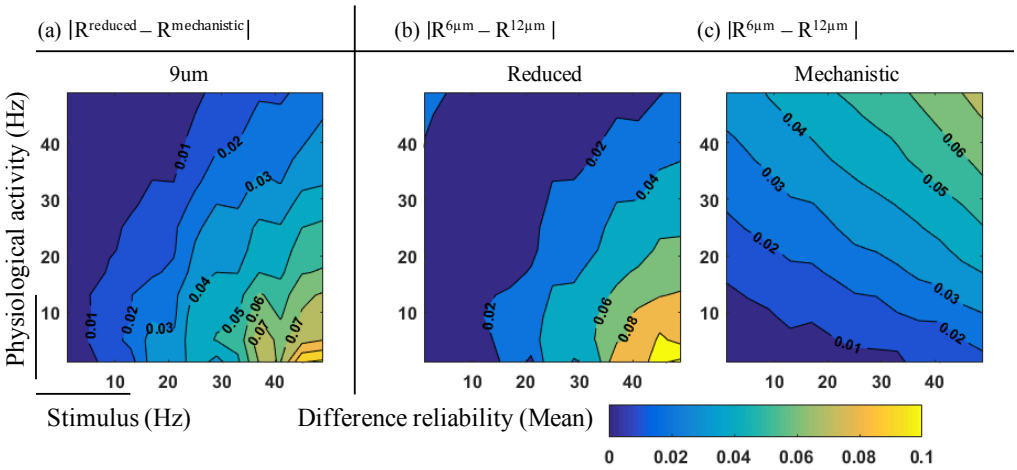

FIGURE 3.2: Influence of diameter on relay reliability. **a**. Relay map of abs(reduced - mechanistic) model for $9\,\mu m$ diameter. **b,c**. Relay map of abs($6\,\mu m$ vs $12\,\mu m$) diameters for reduced and mechanistic models respectively.

1. At low stimulus frequency ($5\,Hz$) and low physiological frequency ($5\,Hz$), the physiological to stimulus loss of excitability (i.e., a physiological AP just activated the fiber and blocks the incoming stimulus AP) is the dominant type of interaction. It accounts for 46% (reduced) and 44% (mechanistic) of the interactions at 1. Percentage end point action potential due to stimulus and physiological activity is around 50% each.

2. At low stimulus ($5\,Hz$) and high physiological ($45\,Hz$) frequencies, the physiological to physiological loss of excitability is maximum. It accounts for 72% (reduced) and 75% (mechanistic) of the interactions at 2. Percentage end point action potential due to physiological activity is much higher compared to that of stimulus activity.

3. At medium stimulus ($25\,Hz$) and medium physiological ($25\,Hz$) frequencies, the physiological to stimulus loss of excitability is maximum. It accounts for 47% (reduced) and 46% (mechanistic) of the interactions at 3. Percentage end point action potential due to stimulus and physiological activity is around 50% each.

4. At high stimulus ($45\,\mathrm{Hz}$) and low physiological ($5\,\mathrm{Hz}$) frequencies, the physiological to stimulus loss of excitability is maximum. It accounts about 56% (reduced) and 58% (mechanistic) of the interactions at 4. Thus at high stimulus frequencies, the reliability is very low. Percentage end point action potential due to stimulus activity is much higher compared to that of physiological activity.

5. At high stimulus ($45\,\mathrm{Hz}$) and high physiological ($45\,\mathrm{Hz}$) frequencies, the physiological to stimulus loss of excitability is maximum. It accounts for 48% (reduced) and 47% (mechanistic) of the interactions at 5. Percentage end point action potential due to stimulus and physiological activity is around 50% each.

The map in Figure 3.4(a,b) indicates the dominant regions of different interactions under consideration for the reduced and mechanistic model, respectively. We see that the physiological–stimulus loss of excitability is the dominating interaction type, covering $> 50\%$ of the map. Collisions occur least often across all points in the relay map region of zero dominance.

Figure 3.5 shows the relative interaction count between the reduced and mechanistic model. We see that, (a) the number of collisions captured by the reduced model is greater than the mechanistic model, (b) the number of physiological–physiological loss of excitability in the reduced versus mechanistic models have a different linear fit for different stimulus frequencies, (c) the number of physiological–stimulus loss of excitability has a same values for both reduced and mechanistic model and (d) the number of stimulus–physiological loss of excitability in the mechanistic model is greater than that of the reduced model.

3.1.5 Selective relay of action potentials

Depending on the physiological origin of the underlying activity, we may want to modulate its relay to the other end of the fiber differently with electrical stimulation.

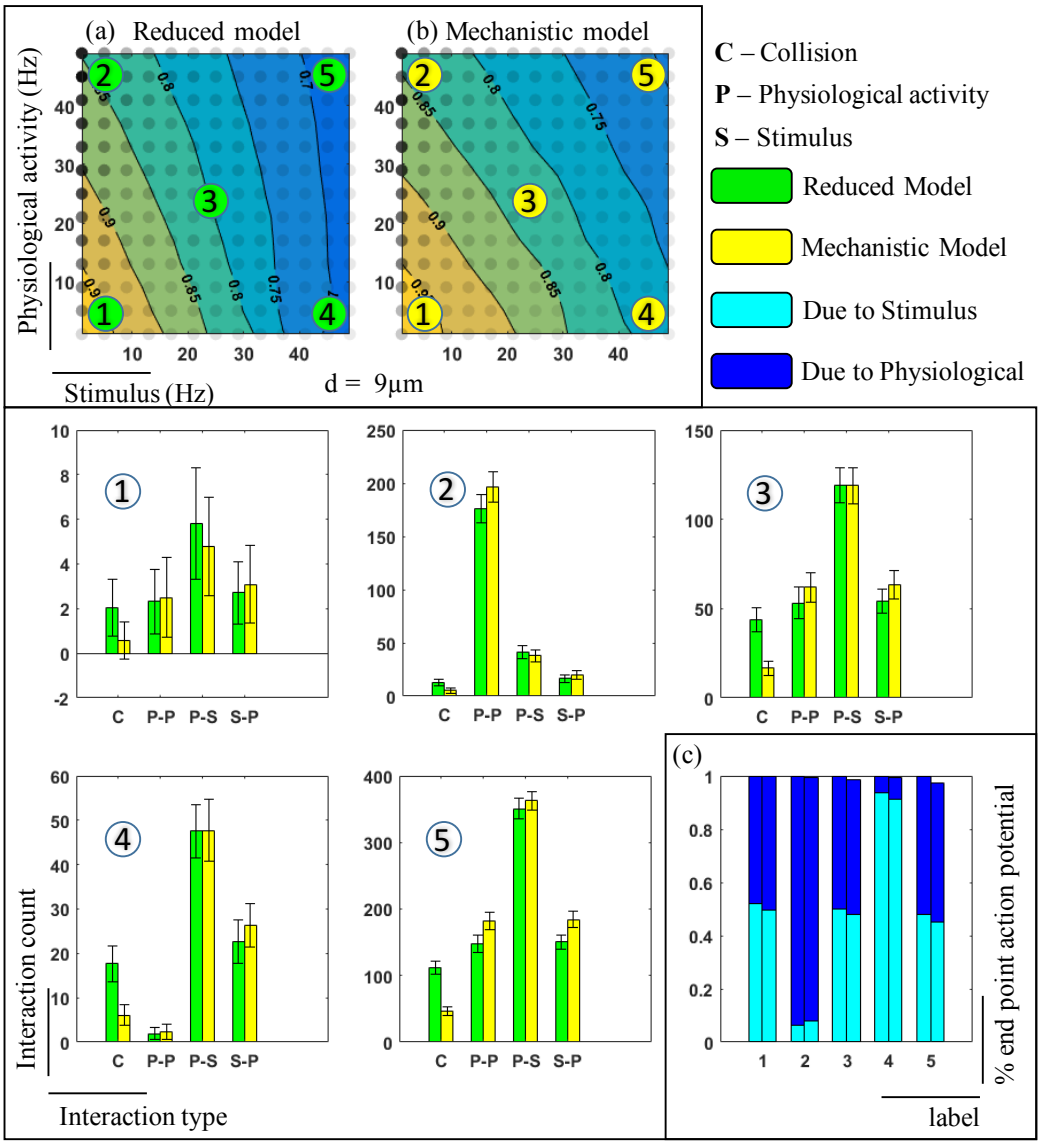

FIGURE 3.3: Interaction statistics at various regions of relay map of 9 µm fiber. **a,b**. Reduced and mechanistic model relay maps for 9 µm diameter nerve fiber. Labels (1)–(5) indicate different regions with green representing reduced model and yellow representing mechanistic model. Each bar group along X-axis represent different interaction type (collision, physiological–physiological, physiological–stimulus, and stimulus–physiological loss of excitability). Y-axis gives mean count of each respective interaction with error bars representing the standard deviation. **c**. Percentage end point action potential due to stimulus (cyan) and underlying physiological activity (blue) at various regions of relay map. First bar in each stacked group represents reduced model and the second group represents the mechanistic model.

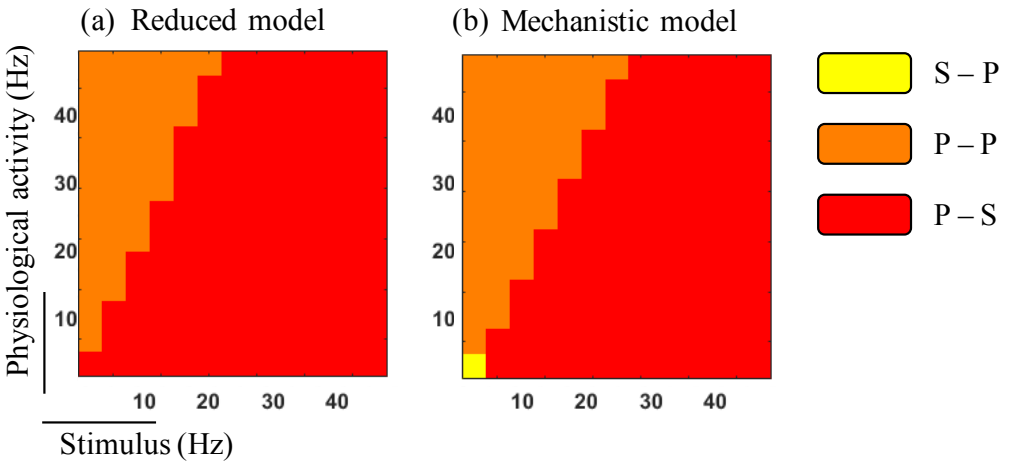

FIGURE 3.4: Dominance of interactions in a relay map. Yellow = stimulus–physiological, Orange = physiological–physiological and Red = physiological–stimulus loss of excitability.

For example, we may want to block pathological activity (e.g., pain), while relaying normal physiological activity (e.g., proprioception or mechanoreception) in neighboring fibers also affected by the electric field. To achieve this objective, we define the following selective relay performance metric:

$$SR(\lambda_{\text{pain}}, \lambda_{\text{phys}}) = \mathrm{R}^{\text{phys}} \times [1 - \mathrm{R}^{\text{pain}}],$$

SR is the product of relay reliability of physiological information and the blocking of pathological signals. We are interested in maximizing the physiological AP relay while minimizing the pathological AP relay. Thus, our goal is to maximize SR with appropriately tuned stimulation. We consider the frequency of pathological signal to be low (1–50 Hz), medium (51–150 Hz), or high (151–200 Hz). Physiological signal input is low (1–50 Hz). Figure 3.6 shows this analysis for a $9\,\mu\text{m}$ diameter nerve fiber.

- *Low pain frequency* (1–50 Hz): SR increases to reach a maximum value of 0.25. After reaching the maximum value, there is a localized decrease in performance. We see that the maximum SR occurs at stimulation frequencies $75\,\text{Hz}$ and $150\,\text{Hz}$.

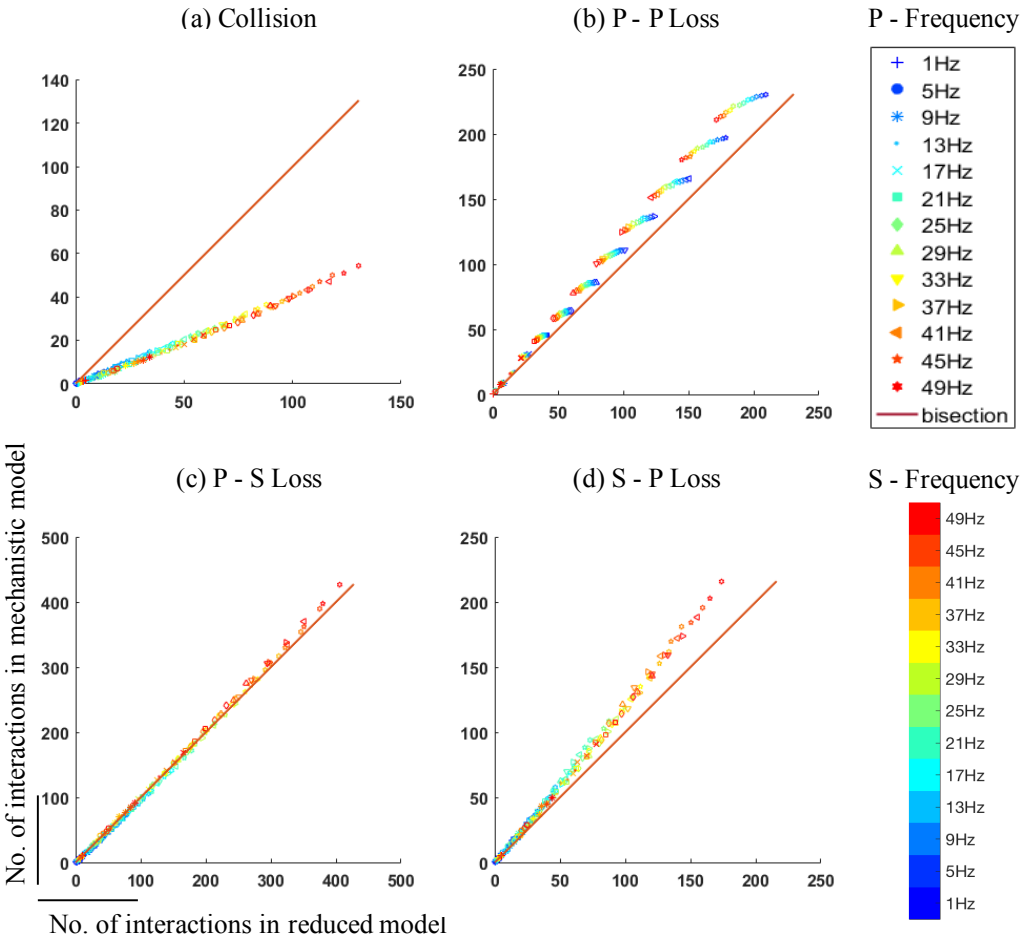

FIGURE 3.5: Scatter plots of interactions for reduced vs mechanistic model. X-axis represents number of interactions in reduced model, Y-axis represents number of interactions in mechanistic model. a = Collision, b = Physiological–Physiological, c = Physiological–Stimulus, d = Stimulus–Physiological loss of excitability. Shapes represent various physiological frequencies. Colors represent various stimulus frequencies. X=Y line shows the bisection.

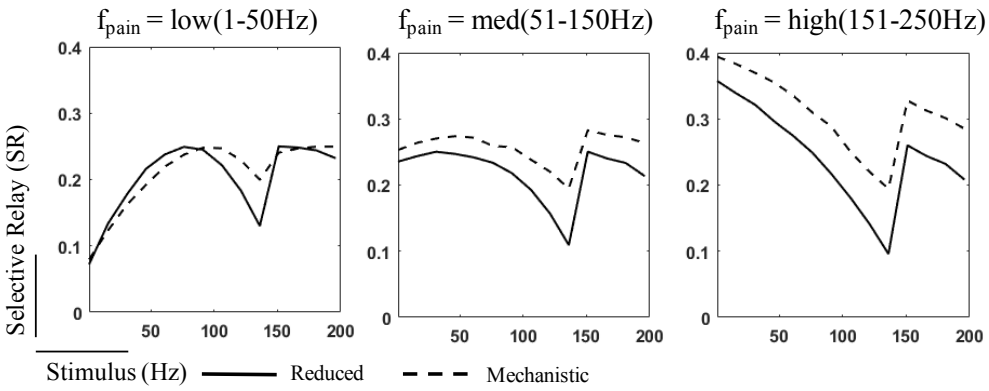

FIGURE 3.6: Selective relay of action potential. Here we considered $9\,\mu\mathrm{m}$ diameter nerve fiber and plot the average SR value for reduced (thick) and mechanistic model (dashed).

- *Medium pain frequency* (51–150 Hz): We see a similar trend in SR values as in the low pain frequency case. The maximum SR value is around 0.3 and is achieved at $50\,\mathrm{Hz}$ and $120\,\mathrm{Hz}$ stimulation.
- *High pain frequency* (151–200 Hz): SR starts high for low stimulus frequencies and then decreases to a minimum, but then increases again after the zero band. The maximum SR value is around 0.4 is achieved at $1\,\mathrm{Hz}$ stimulation.

3.2 Probabilistic vs Mechanistic

In this section, we show results of our stimulation test beds for a monopolar electrode placed $3.5\,\mathrm{mm}$ from the center of a $10\,\mathrm{cm}$-long nerve fiber. We consider three different diameters of nerve fibers in our simulations (6, 9 and $12\,\mu\mathrm{m}$). The results presented in this section are drawn from 50 simulations for each frequency pair (physiological, stimulus) of this model with a stochastic Poisson physiological input. All the mechanistic model simulations were performed on NEURON simulation environment Hines and Carnevale (1997). Analysis of data and probabilistic model simulations were performed on MATLAB, MathWorks.

3.2.1 Relay reliability: Probabilistic vs Mechanistic model

Figure 3.7 shows examples of a physiological relay map for probabilistic and mechanistic model for three different diameters (6, 9 and 12 µm). We see that at low stimulation and physiological frequencies (1–10 Hz), reliability is almost 1 (100%) and thee is more agreement bwteeen the two models. As the stimulus frequency increases, reliability decreases. Also, the probabilistic model captures relay properties that the mechanistic model captures in significantly less run time and with less computational power. Although the values captured by the probabilistic model is much different comapred to mechanistic model. As the axon diameter increases from 6 µm to 12 µm the reliability value increases at each frequency pair.

3.2.2 Influence of fiber diameter on relay reliability

For different fiber diameters, the relay maps change (see Figure 3.7). We observe a horizontal shift in the pattern as we go from 6–12 µm diameter fibers. Consider a stimulus frequency of 50 Hz and physiological frequency of 10 Hz, we see that the relay values for 12 µm is greater than that of 9 µm which is greater than 6 µm (12 µm $>$ 9 µm $>$ 6 µm). This is because of the low conduction velocity of AP's in small fibers. With an increase in fiber diameter, relay reliability increases as the interactions are reduced at higher conduction velocities. Figure 3.8(b,c) shows the difference between the relay maps of 6 µm and 12 µm diameter fibers for probabilistic and mechanistic models.

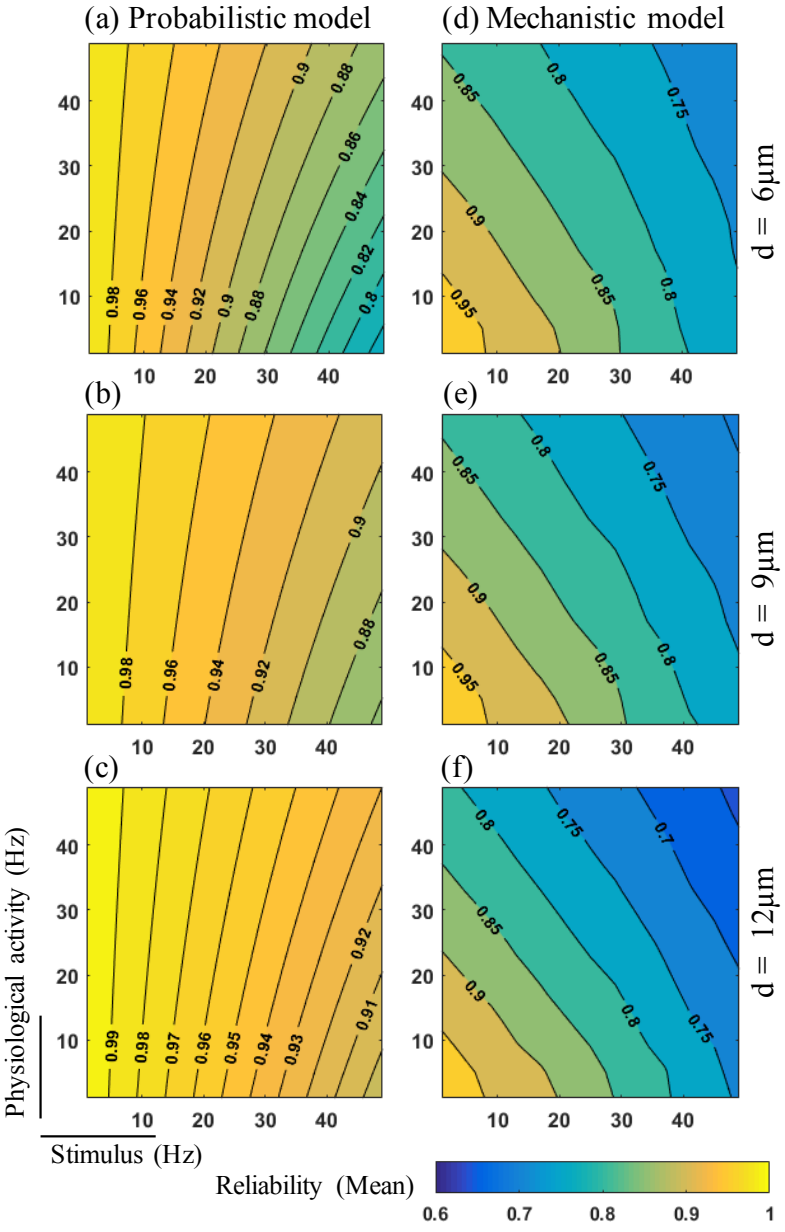

FIGURE 3.7: Physiological reliability maps of probabilistic and mechanistic model for 6, 9 and 12 µm diameters. Contour map of reliability values for a range (1–50 Hz) of physiological frequency (Y-axis) and stimulus frequency (X-axis). Color gradient represents the mean of reliability values (0.6–1).

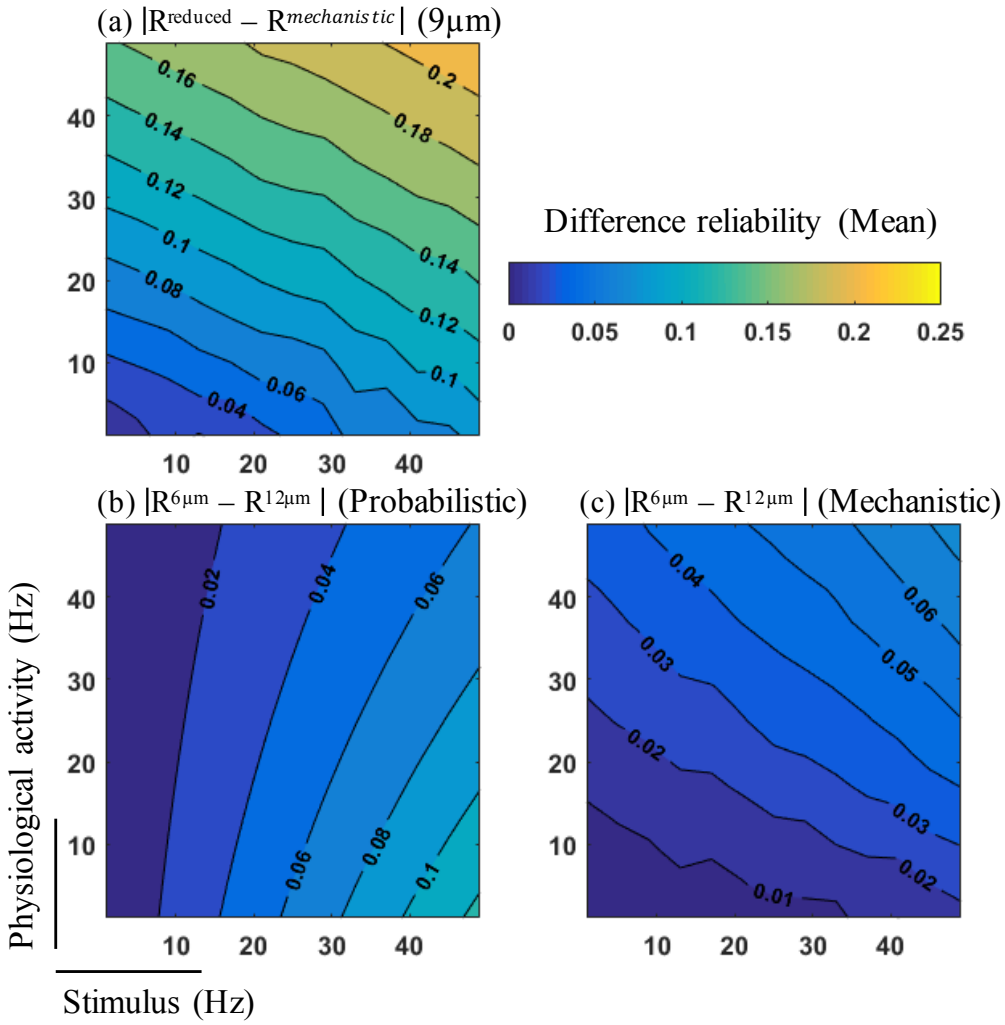

FIGURE 3.8: Influence of diameter on relay reliability. **a**. Relay map of abs(reduced - mechanistic) model for 9 µm diameter. **b,c**. Relay map of abs(6 µm vs 12 µm) diameters for probabilistic and mechanistic models respectively.

4 Discussion

In this work, we study the interactions between electrical stimulation and physiological activity induced action potentials in a mammalian nerve fiber. To achieve this, we construct two different models of a nerve fiber of varying degrees of complexity and realism (reduced and mechanistic) each receiving two inputs: the external stimulus at the middle of the fiber and the underlying physiological activity at one end of the fiber. We administer a periodic pulse train as the stimulus input with frequency ranging between 1–$50\,\mathrm{Hz}$, and the physiological input is drawn from a Poisson distribution with an average spiking rate ranging between 1–$50\,\mathrm{Hz}$. For each frequency pair, we compute the relay reliability as a ratio of the number of physiological to stimulus APs making it to the other end of the fiber over the total number of physiological and stimulus APs generated. We found that relay reliability depends on stimulus frequency and physiological parameters such as frequency and diameter of the nerve fiber, both affecting the interactions between APs generated by both inputs. Different types of interactions (e.g., collisions) were quantified between simulation-evoked activity and underlying physiological activity.

4.1 Comparing the reduced and mechanistic model and the influence of interactions

4.1.1 Relay reliability

The reduced model captures many relay properties that the mechanistic model captures, but with significantly less time and less computation power. This is because the mechanistic model involves solving multi-dimensional differential equations at each fiber node to compute signal transmission. In contrast, the reduced model uses the activation threshold, speed of conduction, and refractory periods to compute relay statistics.

The relay maps for the reduced and mechanistic models are very similar for low input frequencies (see Figure 3.2(a), Figure S2(a)) and begin to differ at higher stimulus frequencies. As expected, we found that the relay reliability is high at low physiological and stimulus frequencies, because fewer interactions between simulation-evoked activity and underlying physiological activity occur. As the frequencies of stimulus and physiological inputs increase, relay reliability decreases (Crago and Makowski 2014). This is due to the increase in number of interactions. The zero band in supplementary simulations (Figure S1) is significant as the nerve fiber no longer responds to the stimulation and underlying physiological activity. We speculate that the stimulation frequency in the zero band resembles that of a "zero" of a linear time invariant transfer function which "absorbs" any incoming physiological AP leading to zero band.

The differences between the reduced and mechanistic model at high frequency stimulation suggest that fiber behavior cannot be quantified by the collision - loss of excitability model at high frequencies, but involves more interactions. Although a limitation to the work presented here, adding more interactions into the reduced model will allow us to make the model better in future studies.

4.1.2 Influence of fiber diameter on relay reliability

We see from Figure 3.2(b,c), that increasing the diameter of the nerve fiber from $6\,\mu\mathrm{m}$ to $12\,\mu\mathrm{m}$ shifts the relay map to the right. This is evident if we look at the zero band (Figure S1), which shifts from $100\,\mathrm{Hz}$ to $150\,\mathrm{Hz}$. This is expected, since the conduction speeds are higher in a bigger fiber (Hursh 1939), and therefore requires a higher frequency stimulus to achieve the relay properties observed for lower stimulus frequencies in smaller fibers.

4.1.3 Interactions along the fiber

We compared different interactions at low, medium, and high physiological–stimulus frequency pairs. For this analysis, we used the data from reduced and mechanistic model simulation of $9\,\mu\mathrm{m}$ diameter fiber. Figure 3.3(1) shows that at low physiological ($< 30\,\mathrm{Hz}$) and stimulus frequencies (1–$50\,\mathrm{Hz}$), the physiological–stimulus loss of excitability has the largest interaction count. In general, the inter signal loss of excitability is dominant. Collisions are the least frequent interaction type (Crago and Makowski 2014).

The physiological–stimulus refractory period is much larger when compared to the stimulus–physiological refractory period, resulting in a higher loss of APs in the former (see Table. 3.1). Increasing the physiological frequency ($45\,\mathrm{Hz}$) while keeping the stimulus low ($5\,\mathrm{Hz}$) results in high physiological–physiological interaction. When both physiological and stimulus frequencies are high, we see high physiological–stimulus loss. This is surprising as we expected to see a high intra signal loss here. As mentioned earlier, long refractoriness in the nerve fiber from physiological–stimulus loss leads to more interactions. The percentage of end point action potentials due to stimulus and physiological activity along the $f_{stim} = f_{phys}$ line is around 50% each. This is similar to the results seen in (Crago and Makowski

2014). For high and low f_{stim}/f_{phys} ratio, the percentage is dominated by the higher frequency input.

As illustrated in Figure 3.5, we compared interaction statistics generated from the reduced and mechanistic models. We see that both have comparable statistics, although the mechanistic model generates fewer collisions compared to the reduced model. When we capture collisions in the reduced model, we assume that a physiological AP (t_1) collides with stimulus AP (t_2) if the physiological AP falls in the range of $[t_2 - i, t_2 + i]$, where i depends on speed of conduction of the fiber and its length. This might not be the case in mechanistic model. This range may be smaller which results in fewer collisions.

4.1.4 Experimental efforts to study interactions on nerve fiber

It is worth mentioning a few experimental studies that investigate and/or exploit interactions between a stimulus generated AP and underlying physiological activity. Collision block was used in cats as a technique to isolate a single unmyelinated nerve fiber from vagal afferent fibers (Iggo 1958). Iggo stimulated the fiber at both ends and studied collisions between antidromic activation from one end with orthodromic activation from other end. Collision block was also exploited to artificially block unwanted physiological activity in the sciatic nerve (van den Honert and Mortimer 1981). A periodic train of unidirectional antidromic action potentials were used to block ongoing orthodromic activity. These studies considered only collisions and the studies were limited to deterministic inputs (single pulse or periodic train of impulses).

4.2 Comparing the probabilistic and mechanistic model and the influence of interactions

4.2.1 Relay reliability

The probabilistic model captures many relay properties that the mechanistic model captures, but with significantly less time and less computation power. This is because the mechanistic model involves solving multi-dimensional differential equations at each fiber node to compute signal transmission. In contrast, the probabilistic model uses the fiber length, speed of conduction, and refractory periods to compute relay statistics.

As expected, we found that the relay reliability is high at low physiological and stimulus frequencies, because fewer interactions between simulation-evoked activity and underlying physiological activity occur. As the frequencies of stimulus and physiological inputs increase, relay reliability decreases. This is due to the increase in number of interactions. The differences between the probabilistic and mechanistic model at high frequency stimulation suggest that fiber behavior cannot be quantified by the collision - loss of excitability model, but involves more interactions. In the future, we plan (i) to consider more complex physiological inputs than Poisson, such as doublets or bursts, (ii) to add more interactions into the existing probabilistic model.

4.2.2 Influence of fiber diameter on relay reliability

We see from Figure 3.8(b,c), that increasing the diameter of the nerve fiber from $6\,\mu\mathrm{m}$ to $12\,\mu\mathrm{m}$ shifts the relay map to the right. This is expected, since the conduction speeds are higher in a bigger fiber Hursh (1939), and therefore requires a higher frequency stimulus to achieve the relay properties observed for lower stimulus frequencies in smaller fibers.

4.3 Selective Relay

Choosing the optimal set stimulation parameters is critical in electrical nerve stimulation to treat any sensory or motor dysfunctions. Studies have been conducted to optimize the stimulus electrode location (Crago and Makowski 2014, Grill and Mortimer 1998) and frequency (Palmer *et al* 1999, Hamza *et al* 1999). Although nerve fiber interaction based studies to optimize stimulation frequency are limited.

Electrical stimulation of dorsal column fibers is used to alleviate chronic pain (CP) (Shealy *et al* 1967, Wall and Sweet 1967, Stidd *et al* 2012). Critical to advancing CP treatment is a deeper mechanistic understanding of pain transmission and modulation under both normal and pathological conditions, which remain largely elusive because the pain system is complex and builds on a tightly regulated dynamical crosstalk between the peripheral nervous system and the brain via the spinal cord. Under trauma or injury, painful stimuli picked up by peripheral nociceptors and generate action potentials (APs) that travel through the peripheral Aδ-fibers (fast) and C-fibers (slow) into the dorsal root ganglion (DRG). These pain signals then travel up the spino-thalamic tract via projection neurons to reach the supraspinal centers, where pain is ultimately perceived. On the other hand, physiological stimuli such as touch and proprioception are picked up by peripheral innocuous receptors which generate APs that travel through the peripheral Aα- and Aβ-fibers into the dorsal horn. These physiological signals then travel up the dorsal column in medial lemniscus pathway to reach the thalamus and sensory cortex. Under normal conditions, both pain and physiological pathways mediate information in a relatively independent fashion. However, under pathological conditions physiological pathways may pick up pain signals. Recent studies suggest that, under a sensitized condition (see Figure 4.1), A-fiber mechanoreceptors gain abnormal access to the nociceptive pathway and can induce pain (Baron 2009, Song *et al* 2012). When electrical stimulation is applied to dorsal column, we end up affecting both pain and physiological pathways. Ideally, we want to selectively block pain but relay physiological

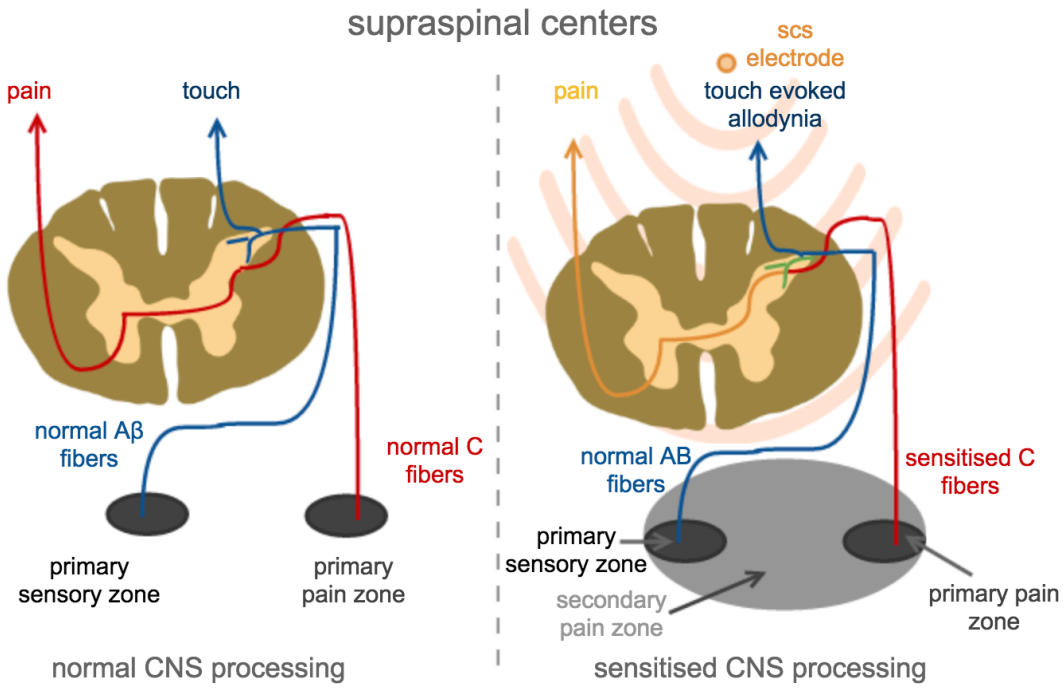

FIGURE 4.1: Pain and sensory signal processing in central nervous system (CNS).

information. This study was motivated in part to achieve this.

When the pain signal is low frequency, SR increases and after reaching a maximum value, there is a localized decrease in SR. We hypothesize that the zero band is responsible for this behavior. We see a similar trend in the medium pain frequency range. Effectively, with a higher pain frequency, it becomes more difficult to block all noxious-related APs. When the pain frequency is high, the SR value is highest when the stimulus frequency is very low. This is because at high pain frequency, most noxious generated APs block themselves out via loss of excitability, resulting in a high SR at low stimulus values. All plots in Figure 3.6 show that a maximum selective relay is achieved at a low-medium frequency of 50–150 Hz, which is, interestingly, what is conventionally used in clinical practice treating CP with peripheral nerve or and spinal cord stimulation (Meyerson and Linderoth 2006, Lind *et al* 2007, Yang *et al* 2011).

4.4 Future Work

In our study, we constructed the underlying physiological activity as a Poisson process, with a mean firing rate of 1–50 Hz (1–200 Hz for simulations in supplementary information). Although Poisson is a representation of action potential arrivals, the same mean firing rate can be obtained from infinitely-many different spike train patterns. Variable patterns (like bursts etc.) may be more realistic characterizations of physiological response processes (Bruns *et al* 2009). Similarly, stimulation with variable patterns may perform better in some applications. Our reduced model simulation considers only three different interactions (collision, inter signal and intra signal loss of excitability). Adding more interaction types (and nonlinear parameters like a relative refractory period) may add predictive power to the reduced and probabilistic models.

Our simulation test bed is a necessary first step toward a better understanding of the effect of electrical stimulation in relay of action potentials in nerve fibers. In the future, we plan (a) to consider more complex physiological inputs than Poisson, such as doublets or bursts, (b) to derive an analytical expression for the fiber reliability, and (c) to augment multiple fibers to construct complex neural circuits.

A Supplementary information

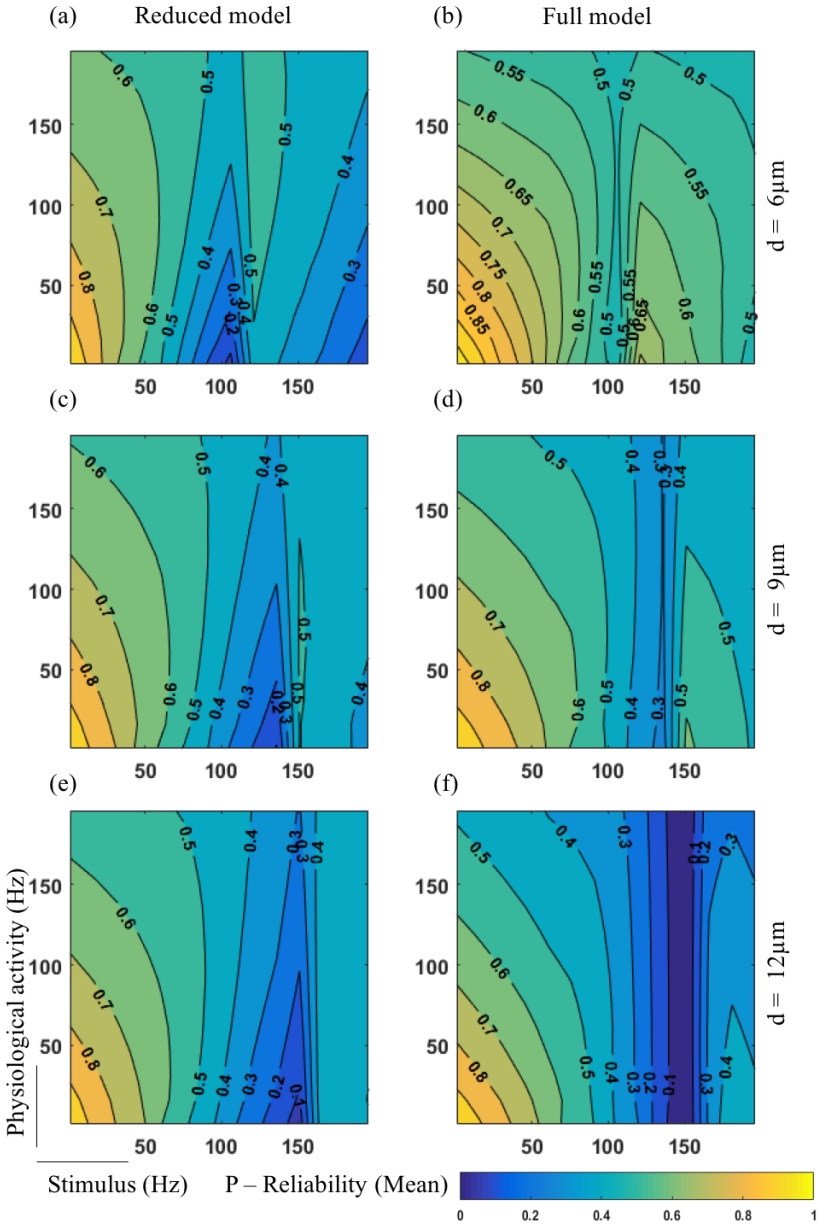

FIGURE A.1: Physiological reliability maps of reduced and full model for 6,9 and 12 µm diameters. Contour map of reliability values for a range (1-200 Hz) of physiological frequency (Y-axis) and stimulus frequency (X-axis). Color gradient represents the mean of reliability values (0-1) with yellow (1) being the highest relay and purple (0) being the lowest.

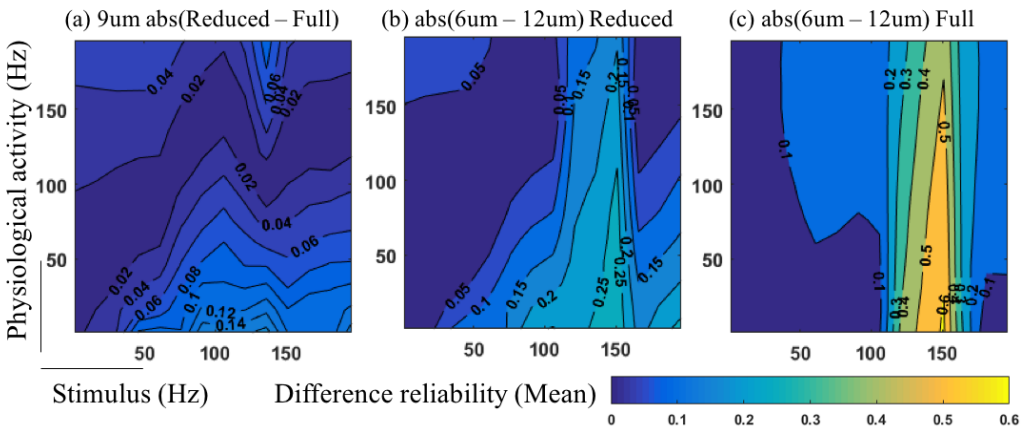

FIGURE A.2: Influence of diameter on relay reliability. **a**. Relay map of abs(reduced - full) model for 9 µm diameter. **b,c**. Relay map of abs(6 µm vs 12 µm) diameters for reduced and full models respectively.

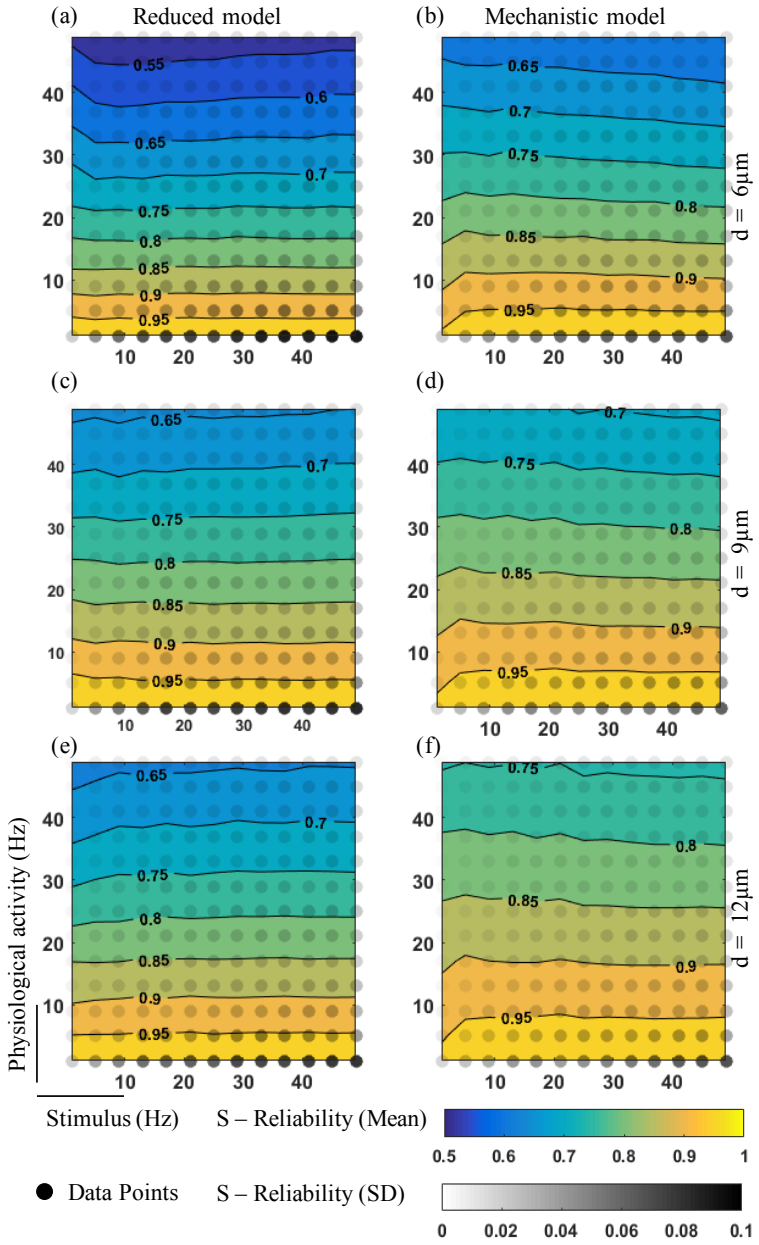

FIGURE A.3: Stimulus reliability maps of reduced and full model for 6, 9 and 12 µm diameters. Contour map of reliability values for a range (1–50 Hz) of physiological frequency (Y-axis) and stimulus frequency (X-axis). Black dots represent the data points. Color gradient represents the mean of reliability values (0.5–1). Grayscale gradient represents the standard deviation (SD) of reliability values (0–0.1).

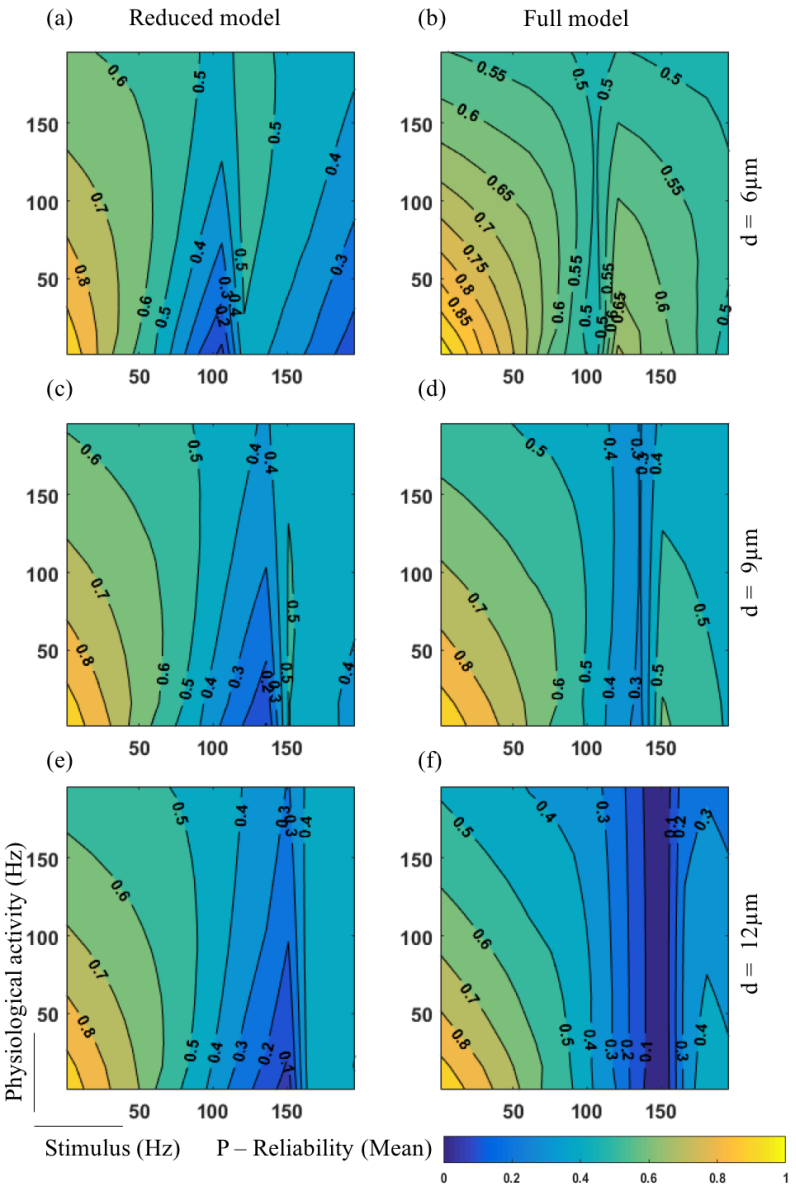

FIGURE A.4: Stimulus reliability maps of reduced and full model for 6,9 and 12 µm diameters. Contour map of reliability values for a range (1-200 Hz) of physiological frequency (Y-axis) and stimulus frequency (X-axis). Color gradient represents the mean of reliability values (0-1) with yellow (1) being the highest relay and purple (0) being the lowest.

Bibliography

Baron, R. (2009). Neuropathic pain: a clinical perspective, *Sensory Nerves*, Springer, pp. 3–30.

Bruns, T. M., Bhadra, N. and Gustafson, K. J. (2009). Bursting stimulation of proximal urethral afferents improves bladder pressures and voiding, *Journal of neural engineering* **6**(6): 066006.

Crago, P. E. and Makowski, N. S. (2014). Alteration of neural action potential patterns by axonal stimulation: the importance of stimulus location, *Journal of neural engineering* **11**(5): 056016.

De Luca, C. J., LeFever, R. S., McCue, M. P. and Xenakis, A. P. (1982). Behaviour of human motor units in different muscles during linearly varying contractions, *The Journal of physiology* **329**(1): 113–128.

Frankenhaeuser, B. and Huxley, A. F. (1964). The action potential in the myelinated nerve fibre of *Xenopus laevis* as computed on the basis of voltage clamp data, *The Journal of Physiology* **171**(2): 302.

Gonzalez-Perez, A., Budvytyte, R., Mosgaard, L. D., Nissen, S. and Heimburg, T. (2014). Penetration of action potentials during collision in the median and lateral giant axons of invertebrates, *Physical Review X* **4**(3): 031047.

Grill, W. M. and Mortimer, J. T. (1998). Stability of the input-output properties of chronically implanted multiple contact nerve cuff stimulating electrodes, *IEEE Transactions on Rehabilitation Engineering* **6**(4): 364–373.

Groves, D. A. and Brown, V. J. (2005). Vagal nerve stimulation: a review of its applications and potential mechanisms that mediate its clinical effects, *Neuroscience & Biobehavioral Reviews* **29**(3): 493–500.

Hamza, M. A., White, P. F., Ahmed, H. E. and Ghoname, E.-s. A. (1999). Effect of the frequency of transcutaneous electrical nerve stimulation on the postoperative opioid analgesic requirement and recovery profile, *Anesthesiology* **91**(5): 1232–1232.

Hines, M. L. and Carnevale, N. T. (1997). The NEURON simulation environment, *Neural computation* **9**(6): 1179–1209.

Hursh, J. B. (1939). Conduction velocity and diameter of nerve fibers, *American Journal of Physiology* **127**(1): 131–139.

Iggo, A. (1958). The electrophysiological identification of single nerve fibres, with particular reference to the slowest-conducting vagal afferent fibres in the cat, *The Journal of physiology* **142**(1): 110.

Jänig, W., Grossmann, L. and Gorodetskaya, N. (2009). Mechano-and thermosensitivity of regenerating cutaneous afferent nerve fibers, *Experimental brain research* **196**(1): 101–114.

Kajander, K. C. and Bennett, G. J. (1992). Onset of a painful peripheral neuropathy in rat: a partial and differential deafferentation and spontaneous discharge in A beta and A delta primary afferent neurons, *Journal of Neurophysiology* **68**(3): 734–744.

Katz, B. (1950). Action potentials from a sensory nerve ending, *The Journal of physiology* **111**(3-4): 248.

Kralj, A. R. and Bajd, T. (1989). *Functional electrical stimulation: standing and walking after spinal cord injury*, CRC press.

Lind, G., Schechtmann, G., Winter, J. and Linderoth, B. (2007). Drug-enhanced spinal stimulation for pain: a new strategy, *Operative Neuromodulation*, Springer, pp. 57–63.

McIntyre, C. C., Richardson, A. G. and Grill, W. M. (2002). Modeling the excitability of mammalian nerve fibers: influence of afterpotentials on the recovery cycle, *Journal of neurophysiology* **87**(2): 995–1006.

McNeal, D. R. (1976). Analysis of a model for excitation of myelinated nerve, *IEEE Transactions on Biomedical Engineering* **23**(4): 329–337.

Medtronic Neuromodulation (2007). *Technical design summary: Model 39565 specify 5-6-5 surgical lead*.

Meyerson, B. A. and Linderoth, B. (2006). Mode of action of spinal cord stimulation in neuropathic pain, *Journal of pain and symptom management* **31**(4): S6–S12.

Mortimer, J. T. and Bhadra, N. (2004). Peripheral nerve and muscle stimulation, *Neuroprosthetics: Theory and Practice*, World Scientific, pp. 638–682.

Palmer, S. T., Martin, D. J., Steedman, W. M. and Ravey, J. (1999). Alteration of interferential current and transcutaneous electrical nerve stimulation frequency: effects on nerve excitation, *Archives of physical medicine and rehabilitation* **80**(9): 1065–1071.

Peckham, P. H. and Kilgore, K. L. (2013). Challenges and opportunities in restoring function after paralysis, *IEEE Transactions on Biomedical Engineering* **60**(3): 602–609.

Pfurtscheller, G., Müller, G. R., Pfurtscheller, J., Gerner, H. J. and Rupp, R. (2003). 'Thought'–control of functional electrical stimulation to restore hand grasp in a patient with tetraplegia, *Neuroscience letters* **351**(1): 33–36.

Reilly, J. P. (1989). Peripheral nerve stimulation by induced electric currents: exposure to time-varying magnetic fields, *Medical and Biological Engineering and Computing* **27**(2): 101–110.

Rubinstein, J. T. (1993). Axon termination conditions for electrical stimulation, *IEEE transactions on biomedical engineering* **40**(7): 654–663.

Sacré, P., Sarma, S. V., Guan, Y. and Anderson, W. S. (2015). Electrical neurostimulation for chronic pain: on selective relay of sensory neural activities in myelinated nerve fibers, *Proceeding of the 37th Annual International Conference of the IEEE Engineering in Medicine and Biology Society (EMBC)*, pp. 4705–4708.

Sadashivaiah, V. (2016). Modeling the interactions in a mammalian nerve fiber. **URL:** *https://github.com/vjs347/nerve-fiber-modeling*

Schwarz, J. R., Reid, G. and Bostock, H. (1995). Action potentials and membrane currents in the human node of ranvier, *Pflügers Archiv* **430**(2): 283–292.

Shealy, C. N., Mortimer, J. T. and Reswick, J. B. (1967). Electrical inhibition of pain by stimulation of the dorsal columns: preliminary clinical report., *Anesthesia & Analgesia* **46**(4): 489–491.

Shechter, R., Yang, F., Xu, Q., Cheong, Y.-K., He, S.-Q., Sdrulla, A., Carteret, A. F., Wacnik, P. W., Dong, X., Meyer, R. A. *et al* (2013). Conventional and kilohertz-frequency spinal cord stimulation produces intensity-and frequency-dependent inhibition of mechanical hypersensitivity in a rat model of neuropathic pain, *The Journal of the American Society of Anesthesiologists* **119**(2): 422–432.

Song, Y., Li, H.-M., Xie, R.-G., Yue, Z.-F., Song, X.-J., Hu, S.-J. and Xing, J.-L. (2012). Evoked bursting in injured Aβ dorsal root ganglion neurons: a mechanism underlying tactile allodynia, *Pain* **153**(3): 657–665.

Stidd, D. A., Wuollet, A., Bowden, K., Price, T., Patwardhan, A., Barker, S., Weinand, M. E., Annabi, J. and Annabi, E. (2012). Peripheral nerve stimulation for trigeminal neuropathic pain, *Pain physician* **15**(1): 27.

Struijk, J. J., Holsheimer, J., Van Veen, B. and Boom, H. B. (1991). Epidural spinal cord stimulation: calculation of field potentials with special reference to dorsal column nerve fibers, *IEEE transactions on biomedical engineering* **38**(1): 104–110.

van den Honert, C. and Mortimer, J. T. (1981). A technique for collision block of peripheral nerve: Frequency dependence, *IEEE Transactions on Biomedical Engineering* **5**(BME-28): 379–382.

Wall, P. D. and Sweet, W. H. (1967). Temporary abolition of pain in man, *Science* **155**(3758): 108–109.

Wesselink, W. A., Holsheimer, J. and Boom, H. B. K. (1999). A model of the electrical behaviour of myelinated sensory nerve fibres based on human data, *Medical & biological engineering & computing* **37**(2): 228–235.

Yang, F., Carteret, A. F., Wacnik, P. W., Chung, C.-Y., Xing, L., Dong, X., Meyer, R. A., Raja, S. N. and Guan, Y. (2011). Bipolar spinal cord stimulation attenuates mechanical hypersensitivity at an intensity that activates a small portion of A-fiber afferents in spinal nerve-injured rats, *Neuroscience* **199**: 470–480.

Vijay Sadashivaiah

Research Assistant
Institute of Computational Medicine
Johns Hopkins University
318 Hackerman Hall
3400 N. Charles Street, Baltimore, MD 21218
E-mail: vjs@jhu.edu
Phone: (+1) 443 447-3694
Webpage: http://pages.jh.edu/~vsadash1

EDUCATION

Johns Hopkins University, Baltimore, MD
Master of Science, Biomedical Engineering, Expected May 2017 GPA: 3.8/4.0

Massachusetts Institute of Technology, Cambridge, MA
Visiting Student, Media Arts and Sciences, June – September 2014

PES University, Bangalore, India
Bachelor of Science, Electrical Engineering, May 2015 GPA: 9.32/10.0
(Top 5% of class)

RESEARCH

Neuromedical Control Systems Lab Research Assistant
September 2015 – Present Baltimore, MD
1. Constructing a probabilistic model of nerve fiber to test the performance of Electrical Nerve Stimulation (ENS)
2. My model reduced our codebase by 70% and runs in under 30 minutes, against a mechanistic model which takes a week to simulate in parallel on a 250 node cluster
3. Working on clinical pain data from Johns Hopkins Pain Institute to construct statistical models using generalized linear model (GLM)
4. Amalgamated the findings into a journal paper submitted for publication

Laboratory of Sensory Processing Summer Intern
June 2015 – August 2015 Lausanne, Switzerland
1. Analyzed the neural circuits involved in sensorimotor interactions
2. Data analysis involved 1 TB of voltage sensitive images across multiple trials
3. Techniques involved k-means clustering, matrix manipulation, statistical testing etc
4. Amalgamated the findings into a research paper published in SPIE Neurophotonics

MIT Media Lab – Camera Culture Summer Intern
June 2014 – September 2014 Cambridge, MA
1. Worked on Coded Time Of Flight imaging.
2. Task involved FPGA coding, PCB design, data acquisition and data analysis
3. Authored a do it yourself manual for the camera.
4. Featured on MIT webpage and BBC news.

Healthcare Innovation Lab Research Assistant
June 2012 – May 2014 Bangalore, India
1. Used signal processing techniques learnt in class to analyze real world medical data
2. Projects included time series analysis of EKG, Skin Conductance, ERG signal etc

PUBLICATIONS

Peer Reviewed Journals

[**J1**] **Sadashivaiah, V.**, Sacre, P., Guan, Y., Anderson, W. S., Sarma, S. V.,*Modeling the interactions between electrically and physiologically induced action potentials in a mammalian nerve fiber.* (Submitted)
[**J2**] Kyriakatos A, **Sadashivaiah V**, Zhang Y, Motta A, Auffret M, Petersen CH; Voltage-sensitive dye imaging of mouse neocortex during a whisker detection task. Neurophoton. 0001;4(3):031204.

Conference Proceedings

[**C1**] **Sadashivaiah, V.**, Sacr, P., Guan, Y., Anderson, W. S., Sarma, S. V., *Electrical neurostimulation of a mammalian nerve fibers: A probabilistic versus mechanistic approach.* (Submitted)
[**C2**] Gunnarsdottir, K., **Sadashivaiah, V.**, Kerr, M., Santaniello, S., Sarma, S. V., *Using Demographic and Time Series Physiological Features to Classify Sepsis in the Intensive Care Unit*, 38th Annual International Conference of the IEEE Engineering in Medicine & Biology Society, Florida, 2016.
[**C3**] Das, A., Swedish, T., Wahi, A., Moufarrej, M., Noland, M., Gurry, T., Michel, E. M., Aksel, D., Wagh, S., **Sadashivaiah, V.**, Zhang, X., Raskar, R., *Mobile phone based mini-spectrometer for rapid screening of skin cancer.* Proc. SPIE 9482, Next-Generation Spectroscopic Technologies VIII, 94820M (June 3, 2015).
[**C4**] Pavan, K. R., Rao, S. A., Rao, V. V., Bongale, V. A., *__Sadashivaiah, V.__*, *Real Time Non-Invasive Cardiac Health Monitoring System.* International Conference on Emergency Medical Service Systems and Innovation & Entrepreneurship in Healthcare, AIIMS, New Delhi, India. October 2013. (* Alphabetical order only).

SKILLS

Programming

Matlab (Proficient), Python (Intermediate), C (Prior Experience), R (Beginner), Neuron (Proficient), SQL (Intermediate), HTML (Prior Experience), CSS (Prior Experience), LaTeX(Proficient)

Hardware: FPGA, Arduino, Raspberry Pi
Tools: Microsoft Office, git

AWARDS AND FELLOWSHIPS

2016	Top 10/200+	HopHacks Spring 2016, Baltimore, MD
2015	Top 17/400+	Fully funded masters admit to Johns Hopkins University
2015	Top 20/700+	Summer research fellowship, Lausanne, Switzerland
2014	NA	NSF Funding MIT grant to support my internship
2014	Top 30/600+	Vecna, Code something that matters
2014	Top 7/100+	Vertech City Challenge, Quebec, Canada
2014	Winners	Best student project, IEEE IMPETUS
2013	Top 20/700+	Intel Global Challenge, Berkeley, CA
2013	Semifinalists	Go Green in the City, Paris, France
2013	Winners	Innovation for a better tomorrow, Kerala, India
2011	203/130,000	Engineering entrance test for Karnataka state, India
2011	Top 220/610,000	College tuition support, Government of India
2009	Top 100	International Mathematics Olympiad by SOF

COURSEWORK

Graduate Courses

Learning Theory, Algorithms, Digital Health and Biomedical Informatics, Systems Bioengineering II, Systems Bioengineering III, Auditory Neurophysiology, Topics in Systems Neuroscience, Models of a Neuron, Introduction to Computational Medicine, Neuroscience of Pain.

Undergraduate Courses*

Information Theory, Linear Algebra, Differential Equations, Calculus, Digital Signal Processing, Probability and Random Processes, Applied Mathematics, Signals and Systems, Computer Networks (*Relevant courses only. See transcript for all courses).

Independent courses*

Machine Learning, Computational Neuroscience, Cellular mechanisms of Brain function, Python Programming, Algorithms (*MOOC platform)

TEACHING AND INSTRUCTION

2016	TA	Statistical Mechanics and Thermodynamics
2016	TA	Models and Simulations
2015	TA	Statistical Mechanics and Thermodynamics
2014	Instructor	Big data and Recognition – Khumbthon. Camera Culture, MIT
2014	Instructor	Electrophysiology of Eye – ReDx. Camera Culture, MIT.
2012	TA	Logic Design, PES University

LEADERSHIP

2016	Advocacy Chair	Graduate Representative Organization, JHU
2014	Core team	Circuitus - Hardware Hackathon, PES University
2013	Team Lead	Prakalpa - Science fair, PES University
2012	Core Team	IEEE PES University
2011	PR Head	Sequitur, Science fair, PES University

REFERENCES

Dr. Sridevi V. Sarma
Associate Professor
Department of Biomedical Engineering,
Johns Hopkins University.
Email: sree@jhu.edu
Phone: +1 (410) 516-4381

Dr. Carl Petersen
Full Professor
Laboratory of Sensory Processing,
Department of Life Sciences and Technology,
cole Polytechnique Fdrale de Lausanne.
Email: carl.petersen@epfl.ch
Phone: +41 21 69 31721

Dr. Ramesh Raskar
Associate Professor
Camera Culture group,
Media Arts and Sciences,
Massachusetts Institute of Technology.
Email: raskar@mit.edu,
Phone: +1 (617) 953-9799